EDGE ARTICLE

Check for updates

K₃V₂O₃F₄(IO₃)₃: a high-performance SHG crystal containing both five and six-coordinated V⁵⁺ cations†

Jin Chen, [ID] [abc] Chun-Li Hu, [a] Yi-Lin Lin, [ID] [a] Yan Chen, [ID] [a] Qian-Qian Chen[a] and Jiang-Gao Mao [ID] *[a]

The combination of d⁰ transition metal oxofluorides with iodate anions helps to synthesize polar crystals. Herein, a novel polar crystal, K₃V₂O₃F₄(IO₃)₃, which is the first metal vanadium iodate with two types of V⁵⁺-centered polyhedra (VO₄F₂ octahedron and VO₃F₂ trigonal bipyramid), has been prepared hydrothermally. It crystallizes in the polar space group of *Cmc*2₁ and its structure displays an unprecedented 0D [V₂O₃F₄(IO₃)₃]³⁻ anion, which is composed of Λ-shaped *cis*-[VO₂F₂(IO₃)₂]³⁻ and [VO₂F₂(IO₃)]²⁻ anions interconnected *via* the corner-sharing of one oxo anion. The synergy gained from the VO₄F₂, VO₃F₂ and IO₃ groups resulted in K₃V₂O₃F₄(IO₃)₃ exhibiting both a strong second-harmonic generation (SHG) response (1.3 × KTiOPO₄) under 2050 nm laser irradiation and a large birefringence (0.158 @ 2050 nm). This study provides a facile route for designing SHG materials by assembling various vanadium oxide-fluoride motifs and iodate anions into one compound.

Introduction

Polar crystals are one of the hotspots for scientific investigations, and are urgently needed in the fields of pyroelectrics, ferroelectrics, piezoelectrics and SHG optics. As an input laser passes through an SHG crystal, frequency doubling occurs, which can extend the spectral ranges of the output laser.[1–3] Hence, the SHG crystals play a crucial role in modern laser science and technology. On the other hand, the birefringent crystals that can create and control the polarized light, are also highly needed in the laser industry.[4–6] Notably, SHG efficiency and birefringence are primarily related to the polarization and anisotropic properties of crystal structures.[7–9]

The iodate anion is able to exhibit giant microscopic acentricity owing to the second-order Jahn–Teller (SOJT) distortion induced by the lone-pair electrons of the I⁵⁺ cation.[10–12] Accordingly, the design and synthesis of novel metal iodates with aligned IO₃ groups have attracted tremendous commercial and academic interest. Of great importance are metal iodates which can exhibit high SHG response ($d_{ij} > 10 \times$ KDP) or/and large birefringence ($\Delta n > 0.15$ @ 1064 nm).[13–29] Recently, two

[a]State Key Laboratory of Structural Chemistry, Fujian Institute of Research on the Structure of Matter, Chinese Academy of Sciences, Fuzhou, 350002, P. R. China. E-mail: mjg@fjirsm.ac.cn

[b]College of Chemistry and Materials Science, Fujian Provincial Key Laboratory of Polymer Materials, Fujian Normal University, Fuzhou, 350007, P. R. China

[c]University of Chinese Academy of Sciences, Beijing 100039, P. R. China

† Electronic supplementary information (ESI) available. CCDC 2093711. For ESI and crystallographic data in CIF or other electronic format see DOI: 10.1039/d1sc06026k

new effective routes to high performance metal iodate SHG crystals have been developed. One is using the 2D [Bi₂O₂]²⁺ layer and 3D [BiF₂]⁺ cationic network for the confined iodate anions to be arranged in a favorable additive fashion, which has successfully led to the discovery of BiO(IO₃) (12.5 × KDP)[20] and Bi(IO₃)F₂ (11.5 × KDP, 0.22 @ 1064 nm).[21] On the other hand, the condensation of iodate anions can also lead to the formation of polyiodates with outstanding SHG or birefringence properties, such as GdI₅O₁₄ (15 × KDP)[29] and SrI₂O₅F₂ (0.180 @ 1064 nm).[26]

The V⁵⁺-centered polyhedra feature rich structural configurations and large optical anisotropy. The V⁵⁺ cation can be four, five and six coordinated with tetrahedral, trigonal-bipyramidal and octahedral geometries, respectively. Many metal vanadates featuring an isolated VO₄ tetrahedron are able to display large SHG effects, such as Li₃VO₄ (6 × KDP), LiRb₂VO₄ (5 × KDP) and SrTa₂V₂O₁₁ (0.5 × LiNbO₃).[30–32] Interestingly, K₃V₅O₁₄ (100 × α-SiO₂) contains a 2D [V₅O₁₄]³⁻ layer involving both VO₄ and VO₅ groups.[33] Moreover, introducing the V⁵⁺ cation into metal iodate might help in achieving large SHG effects, hence the vanadyl iodates are an ideal class of materials for the exploration of SHG crystals.[34–42] The VO₄ tetrahedron usually does not link with the IO₃ units directly, so as to form mixed anion compounds. Only Zn₂(VO₄)(IO₃) (6 × KDP) is SHG-active, which features isolated (VO₄)³⁻ and (IO₃)⁻ anions bridged by Zn²⁺ cations.[36] The five-coordinated V⁵⁺ cation can be connected to 1D V-IO₃ chains *via* the bridging of iodate units, such as the 1D [VO₂(IO₃)₂]⁻ chain in NaVO₂(IO₃)₂(H₂O) (20 × KDP, 0.22 @ 1064 nm).[39] Besides, the SOJT effect of the V⁵⁺ cation can lead to the octahedron being distorted toward a corner (C4), an edge

(C2) or a face (C3), such as the VO_5F octahedron (C2 distortion) in $CsVO_2F(IO_3)$ (1.1 × KTP),[34] VO_4F_2 (C3 distortion) in α- and β-$Ba_2[VO_2F_2(IO_3)_2](IO_3)$ (9 × KDP)[35] and VO_6 (C4 distortion) in $K(VO)_2O_2(IO_3)_3$ (3.6 × KTP).[38] So far, however, all of the metal vanadyl iodates reported involve only a kind of V^{5+}-centered polyhedron. It is of great interest but challenging if two different types of V-centered polyhedra can be combined into one metal iodate. In addition, exploring novel SHG materials with unprecedented crystal structures via the substitution and bridging of V-centered oxyfluoride groups such as the VO_4F_2 octahedron in 0D Λ-shaped cis-$[VO_2F_2(IO_3)_2]^{3-}$ polyanions is a facile route.[34,35] We also hope that new SHG-active vanadium iodate-fluorides feature a smaller-dimensional anionic architecture in order to exhibit a larger birefringence.

Our explorations of the $A^+–V^{5+}–(IO_3)^-–F^-$ system have resulted in the discovery of $K_3V_2O_3F_4(IO_3)_3$, which features an unprecedented 0D $[V_2O_3F_4(IO_3)_3]^{3-}$ binucleate polyanion, being composed of both the VO_4F_2 octahedron and VO_3F_2 trigonal-bipyramid. Significantly, $K_3V_2O_3F_4(IO_3)_3$ features a strong SHG effect of 1.3 × KTP under 2050 nm laser irradiation and a large birefringence of 0.158 @ 2050 nm.

Experimental

Materials and synthesis

Caution: *Hydrofluoric acid is toxic and corrosive! It must be handled with extreme caution and appropriate protective equipment and training.*

K_2CO_3 (>98%), V_2O_5 (>98%), HF (48–51%), and H_5IO_6 (98%), were used as purchased from Adamas-beta. Single crystals of $K_3V_2O_3F_4(IO_3)_3$ were obtained via hydrothermal reactions. The starting materials are V_2O_5, (91 mg, 0.5 mmol), K_2CO_3, (124.4 mg, 0.9 mmol), H_5IO_6 (250.8 mg, 1.1 mmol), HF (0.35 mL) and H_2O (1 mL). A mixture of the starting materials was put into Teflon pouches (23 mL) sealed in an autoclave, which was heated at 230 °C for 72 hours and cooled to 30 °C at 4 °C h^{-1}. Yellow brick-shaped crystals of $K_3V_2O_3F_4(IO_3)_3$ were obtained in high yields of ∼85% (based on I). The phase purity of $K_3V_2O_3F_4(IO_3)_3$ was checked by powder-XRD (Fig. S1†). The field-emission scanning electron microscopy (FESEM) analyses of $K_3V_2O_3F_4(IO_3)_3$ revealed the existence of K, V, I and F elements (Fig. S2†), and the molar ratio of K : V : I : F (1 : 64 : 1.53 : 2.46) is consistent with the compositions determined by single-crystal XRD analysis.

Powder X-ray diffraction

Powder X-ray diffraction (PXRD) patterns were recorded on a Rigaku MiniFlex II diffractometer with graphite-monochromated Cu Kα radiation in the 2θ range of 10–70° with a step size of 0.02°.

Energy-dispersive X-ray spectroscopy

Microprobe elemental analyses were performed on a field-emission scanning electron microscope (FESEM, JSM6700F) equipped with an energy-dispersive X-ray spectroscope (EDS, Oxford INCA).

Thermal analysis

Thermogravimetric analysis (TGA) and differential scanning calorimetry (DSC) were performed with a NETZCH STA 449F3 unit under a N_2 atmosphere, at a heating rate of 10 °C min^{-1} in the range from 30 to 1000 °C.

Optical measurements

Infrared (IR) spectra were recorded on a Magna 750 FT-IR spectrometer in the form of KBr pellets in the range from 4000 to 400 cm^{-1}.

Ultraviolet-visible-infrared (UV-vis-IR) spectra in the range of 200–2500 nm were recorded on a PerkinElmer Lambda 950 UV-vis-NIR spectrophotometer. Reflectance spectra were converted into absorption spectra by using the Kubelka–Munk function.[43]

Second harmonic generation measurements

Powder SHG measurements were taken with a Q switch Nd: YAG laser generating radiation at 2.05 μm according to the method of Kurtz and Perry.[44] Crystalline $K_3V_2O_3F_4(IO_3)_3$ samples were sieved into distinct particle-size ranges (45–53, 53–75, 75–105, 105–150, 150–210, and 210–300 μm). Sieved $KTiOPO_4$ (KTP) samples in the same particle-size range were used as references. The SHG response of α-$Ba_2[VO_2F_2(IO_3)_2](IO_3)$,[35] α-$Ba_2[GaF_4(IO_3)_2](IO_3)$[45] and γ-$KMoO_3(IO_3)$[46] was remeasured under the same experimental conditions.

Single crystal structure determination

Single-crystal X-ray diffraction data for the title compound were collected on an Agilent Technologies SuperNova dual-wavelength CCD diffractometer with Mo Kα radiation ($λ = 0.71073$ Å) at 293 K. Data reduction was performed with CrysAlisPro, and the absorption correction based on the multi-scan method was applied.[47] The structure of $K_3V_2O_3F_4(IO_3)_3$ was determined by the direct methods and refined by full-matrix least-squares fitting on F^2 using SHELXL-2014.[48] All of the non-hydrogen atoms were refined with anisotropic thermal parameters. The structure was checked for missing symmetry elements using PLATON, and none were found.[49] The flack factor was refined to be −0.04(3), indicating the correctness of its absolute structure.[50] Crystallographic data and structural refinements of the compound are listed in Table 1, and selected bond distances, as well as bond angles, are listed in Tables S1 and S2.†

Computational method

The electronic structure and optical properties were determined using a plane-wave pseudopotential method within density functional theory (DFT) implemented in the total energy code CASTEP.[51,52] For the exchange and correlation functional, we chose Perdew–Burke–Ernzerhof (PBE) in the generalized gradient approximation (GGA).[53] The interactions between the ionic cores and the electrons were described using the norm-conserving pseudopotential.[54] The following orbital electrons were treated as valence electrons: I-$5s^25p^5$, V-$3s^23p^63d^34s^2$, K-$3s^23p^64s^1$, O-$2s^22p^4$ and F-$2s^22p^5$. The numbers of plane waves

included in the basis sets were determined using the cutoff energy of 850 eV. A Monkhorst–Pack k-point sampling of $2 \times 2 \times 3$ was used to perform numerical integration of the Brillouin zone. During the optical property calculations, more than 900 empty bands were involved to ensure the convergence of linear optical properties and SHG coefficients. The other parameters and convergent criteria are the default values of the CASTEP code.[51,52]

The calculations of second-order NLO properties were based on length-gauge formalism within the independent-particle approximation.[55] We adopted Chen's static formula, which was derived by Rashkeev *et al.*[56] and later improved by Chen's group. The static second-order NLO susceptibility can be expressed as

$$\chi^{\alpha\beta\gamma} = \chi^{\alpha\beta\gamma} \text{ (VE)} + \chi^{\alpha\beta\gamma} \text{ (VH)} + \chi^{\alpha\beta\gamma} \text{ (two bands)}$$

where $\chi^{\alpha\beta\gamma}$ (VE) and $\chi^{\alpha\beta\gamma}$ (VH) contribute to $\chi^{\alpha\beta\gamma}$ from virtual-electron processes and virtual-hole processes, respectively, and $\chi^{\alpha\beta\gamma}$ (two bands) contributes to $\chi^{\alpha\beta\gamma}$ from the two-band processes. The formulae for calculating $\chi^{\alpha\beta\gamma}$ (VE), and $\chi^{\alpha\beta\gamma}$ (VH), are given in ref. 57.

Results and discussion

Crystal structure

$K_3V_2O_3F_4(IO_3)_3$ crystallizes in the polar space group $Cmc2_1$ (no. 36) (Table 1). Compared to previously discovered vanadium iodates, $K_3V_2O_3F_4(IO_3)_3$ exhibits a novel 0D $[V_2O_3F_4(IO_3)_3]^{3-}$ binuclear polyanion, with K^+ ions acting as the counter cations to achieve the charge balance (Fig. 1).

The asymmetric unit of $K_3V_2O_3F_4(IO_3)_3$ contains 2 K, 2 V, 2 I, 2 F, and 8 O atoms, among which the K(1), V(1), V(2), I(2), and O(5)–O(8) atoms lie on the *mirror* plane whereas the remaining atoms are located at the general sites. All of the I^{5+} cations link with three O atoms with the bond lengths ranging from 1.782(6) to 1.882(6) Å and the lone-pair electrons occupy the open side of the IO_3 trigonal pyramid.

Table 1 Crystallographic data for $K_3V_2O_3F_4(IO_3)_3$

Formula	$K_3V_2O_3F_4(IO_3)_3$
Formula weight	867.88
Crystal system	Orthorhombic
Space group	$Cmc2_1$
T (K)	293(2)
a (Å)	11.6073(9)
b (Å)	8.5216(7)
c (Å)	15.0983(12)
V (Å^3)	1493.41(20)
Z	4
D_c (g cm^3)	3.860
μ (mm^{-1})	8.393
Goodness of fit on F^2	1.022
Flack factor	−0.04(3)
R_1, wR_2 $[I > 2\sigma(I)]^a$	0.0272, 0.0655
R_1, wR_2 (all data)^a	0.0286, 0.0664

$^a R_1 = \sum \lVert F_o \rvert - \lvert F_c \rVert / \sum \lvert F_o \rvert$ and w$R_2 = \{\sum w[(F_o)^2 - (F_c)^2]^2 / \sum w[(F_o)^2]^2\}^{1/2}$.

Crystal structure
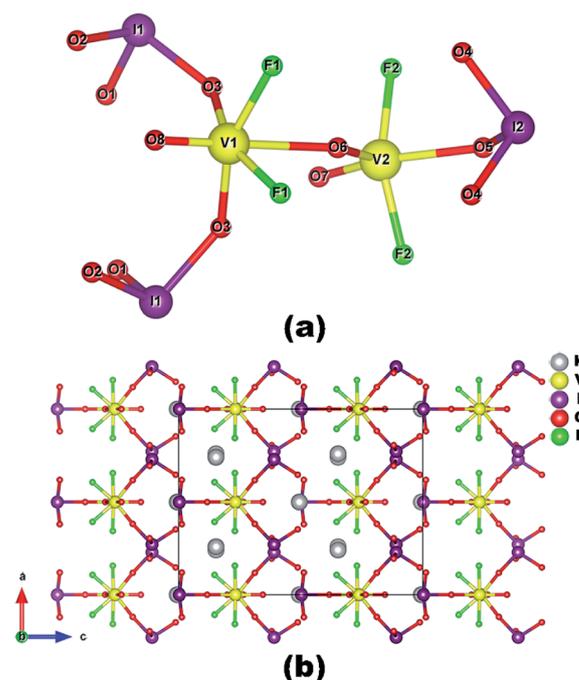
Fig. 1 View of the structures 0D $[V_2O_3F_4(IO_3)_3]^{3-}$ polyanion (a) and $K_3V_2O_3F_4(IO_3)_3$ along the b-axis (b).

The V(1) atom links with two oxo, two fluoride and two iodate anions to form a Λ-shaped *cis*-$[VO_2F_2(IO_3)_2]^{3-}$ polyanion (Fig. 1a). Within the V(1)O_4F_2 polyhedron, there are one short (1.576(10) Å) and one long (2.311(9) Å) V–O bonds as well as four normal (1.872(6) Å for V–O; 1.872(5) Å for V–F) bonds (Fig. S3a†). The *cis*- and *trans*-O/F–V(1)–O/F bond angles are in the range of 79.0(2)–101.7(3)° and 158.2(3)–178.9(4)°, respectively. Hence, the coordination geometry of the V(1)$^{5+}$ cation is a distorted octahedron ($C4$ direction). The distortion magnitude, Δd is defined as the difference in the diagonal bond lengths divided by the cosine of the related angle. The Δd of the VO$_4$F$_2$ octahedron in $K_3V_2O_3F_4(IO_3)_3$ was calculated to be 0.74, which is larger than that of VO$_6$ (0.62, $C4$ direction) in K(VO)$_2$O$_2$(IO$_3$)$_3$,[38] but smaller than those of the VO$_4$F$_2$ octahedron (1.20, $C3$ direction) in α-Ba$_2$[VO$_2$F$_2$(IO$_3$)$_2$](IO$_3$)[35] and VO$_5$F (1.23, $C2$ direction) in CsVO$_2$F(IO$_3$).[34]

The V(2) atom is five-coordinated by two oxo, two fluoride anions, and one oxygen atom from an iodate anion (Fig. 1a). Within the V(2)O_3F_2 group, there are two short (1.633(9) and 1.700(9) Å) and one long (2.032(8) Å) V–O bonds as well as two normal (1.856(6) Å) V–F bonds (Fig. S3b†). The O–V(1)–O bond angles are in the range of 102.9(4)–150.3(4)° and the F–V(1)–F bond angle is 155.7(3)°. Hence, the V(2)O_3F_2 group can be described as a distorted tetragonal pyramid, which is similar to VO$_4$F in β-Ba[VFO$_2$(IO$_3$)$_2$].[35]

The Λ-shaped *cis*-$[VO_2F_2(IO_3)_2]^{3-}$ anion and the $[VO_2F_2(IO_3)]^{2-}$ anion are bridged *via* the corner-sharing (O(6)) into a unique 0D $[V_2O_3F_4(IO_3)_3]^{3-}$ polyanion (Fig. 1a). The 0D

$[V_2O_3F_4(IO_3)_3]^{3-}$ anion can also be regarded as a binuclear $[V_2O_3F_4]$ corner-sharing with three iodate anions, two on the six-coordinated V(1) center and one on the five-coordinated V(2) center. All of the K^+ ions act as spacers between $[V_2O_3F_4(IO_3)_3]^{3-}$ polyanions and maintain charge balance. K(1) is eight coordinated by one VO_4F_2 octahedron in a bidentate fashion (2F) and three IO_3^- units also in a bidentate fashion, whereas the K(2) atom is seven-coordinated by two oxygen atoms from two IO_3^- anions, one F and one O from a VO_4F_2 octahedron, and three F from one VO_4F_2 and two VO_3F_2 units (Fig. S4†). The K–F and K–O bond lengths are in the ranges of 2.621(6)–2.736(6) Å and 2.720(6)–3.067 (8) Å, respectively. The values of bond valence sum (BVS) are calculated to be 1.048, 0.962, 5.051, 4.794, 4.973, and 4.801 for K(1), K(2), V(1), V(2), I(1) and I(2), respectively, showing that their oxidation states are +1, +5 and +5.

Structural comparison

It is interesting to note that both the $[V_2O_3F_4(IO_3)_3]^{3-}$ anion in $K_3V_2O_3F_4(IO_3)_3$ and $[VO_2F(IO_3)]^-$ anion in $CsVO_2F(IO_3)$ can be related to the 0D Λ-shaped cis-$[VO_2F_2(IO_3)_2]^{3-}$ unit in α-Ba$_2$[VO$_2$F$_2$(IO$_3$)$_2$](IO$_3$), the first example of a metal vanadium iodate-fluoride.[35] For the structural transformation from α-Ba$_2$[VO$_2$F$_2$(IO$_3$)$_2$](IO$_3$) to $CsVO_2F(IO_3)$, the 0D $[VO_2F_2(IO_3)_2]^{3-}$ units are changed into 0D $[VO_3F_4(IO_3)_2]^{4-}$ units via the replacement of one F with one O atom, and then the neighboring 0D Λ-shaped units are bridged via the connections of axial oxide and iodate anions.[34] However for $K_3V_2O_3F_4(IO_3)_3$, one $(IO_3)^-$ group in one half 0D $[VO_2F_2(IO_3)_2]^{3-}$ unit was omitted, while the other half 0D $[VO_2F_2(IO_3)_2]^{3-}$ unit sustains the Λ-shaped configuration, and

then such different neighboring 0D units are connected via the corner-sharing of one oxide anion only. Hence, the dimensionality of the $[V_2O_3F_4(IO_3)_3]^{3-}$ anion in $K_3V_2O_3F_4(IO_3)_3$ is smaller than that of the $[VO_2F(IO_3)]^-$ anion in $CsVO_2F(IO_3)$ (0D vs. 3D).

Thermal and optical properties

The thermogravimetric (TG) analyses revealed that $K_3V_2O_3F_4(IO_3)_3$ is thermally stable up to 220 °C (Fig. 2a). The IR spectrum of $K_3V_2O_3F_4(IO_3)_3$ indicates that the sharp absorption peaks mostly appear in the range of 400–1025 cm^{-1}, which can be assigned to the V–O vibrations (824–994 cm^{-1}) and I–O vibrations (411–783 cm^{-1}) (Fig. S5†).[34,35] The UV-vis-IR spectrum shows that $K_3V_2O_3F_4(IO_3)_3$ has a bandgap of 2.40 eV related to the absorption edge of 485 nm (Fig. 2b).

SHG properties

Under 2050 nm laser irradiation, $K_3V_2O_3F_4(IO_3)_3$ displays a very strong SHG signal, which is 1.3 times as large as that of KTP with a particle size of 150–210 μm. Furthermore, it is type-I phase-matchable (Fig. 2c and d). Compared to the metal iodates with Λ-shaped motifs such as $K_5(W_3O_9F_4)(IO_3)$ (1.0 × KTP),[16] α-Ba$_2$[GaF$_4$(IO$_3$)$_2$](IO$_3$) (0.4 × KTP)[45] and γ-KMoO$_3$(IO$_3$) (1.1 × KTP)[46] as well as the crystals containing different V-centered polyhedra such as $K_3V_5O_{14}$ (100 × α-SiO$_2$)[33] and Pb$_2$(V$_2$O$_4$F)(VO)$_2$(SeO$_3$)$_3$ (0.3 × KDP),[58] $K_3V_2O_3F_4(IO_3)_3$ features a higher SHG performance.

It is interesting to compare the SHG effect of $K_3V_2O_3F_4(IO_3)_3$ with previously reported vanadium iodates (Table S3†). The SHG
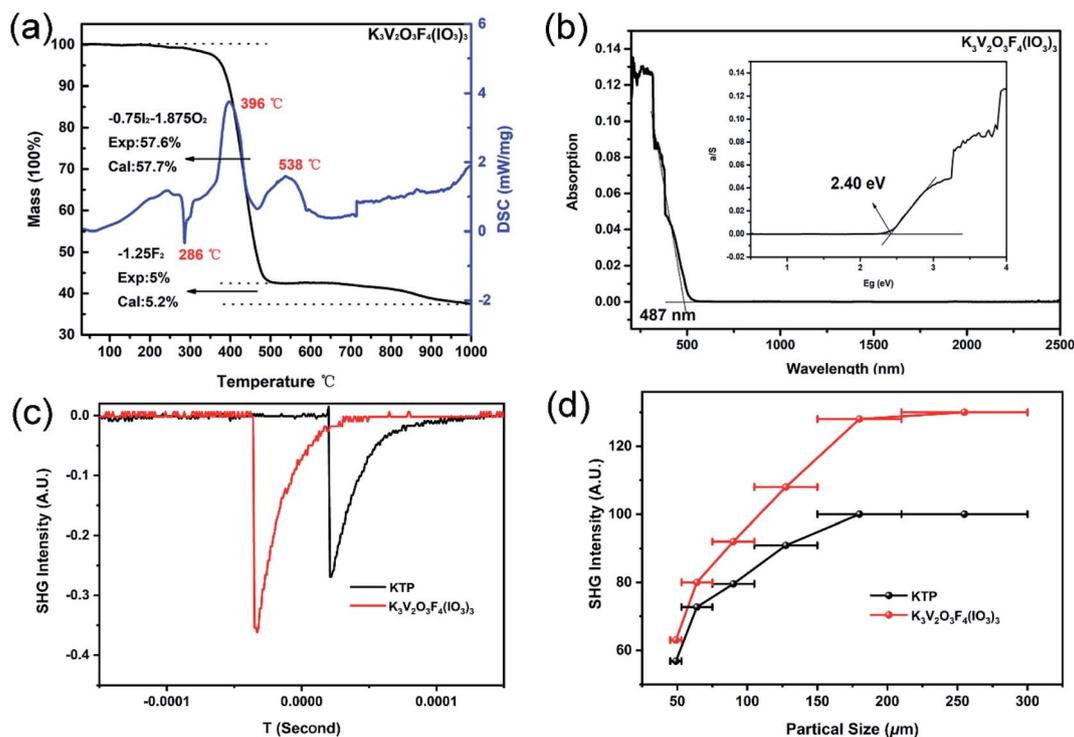

Fig. 2 The TG-DSC curves (a), the UV-vis-IR spectrum (b), the measured oscilloscope traces of the SHG signals (150–210 μm) (c) and SHG intensity vs. particle size of compounds under 2050 nm laser irradiation (d). KTP served as the reference.

response of $K_3V_2O_3F_4(IO_3)_3$ is stronger than that of other metal vanadium iodate-fluorides such as α-Ba$_2$[VO$_2$F$_2$(IO$_3$)$_2$](IO$_3$) (0.7 × KTP) and CsVO$_2$F(IO$_3$) (1.1 × KTP).[34,35] However, compared with K(VO)$_2$O$_2$(IO$_3$)$_3$, $K_3V_2O_3F_4(IO_3)_3$ features a smaller SHG effect (1.3 vs. 3.6 × KTP), which can be attributed to the well-arranged VO$_6$ octahedra and IO$_3$ groups in the 1D [(VO)$_2$O$_2$(IO$_3$)$_3$]$^-$ chain in K(VO)$_2$O$_2$(IO$_3$)$_3$. Hence, we consider that the ideal alignment of vanadium oxide-fluoride and iodate anions may lead to an outstanding SHG effect, which is an effective route for the exploration of high-performance SHG crystals.

Structure–property relationship analysis

The calculation of the band structure showed that $K_3V_2O_3F_4(IO_3)_3$ is an indirect bandgap compound with a bandgap of 2.212 eV, which is smaller than the 2.40 eV from our UV-vis-IR measurements (Fig. 3a). Therefore, a small scissor of 0.188 eV was used for the more accurate description of optical properties.

The partial density of states (PDOS) graph of $K_3V_2O_3F_4(IO_3)_3$ is shown in Fig. S6.† The highest valence band (VB) is occupied by the O-2p states whereas the lowest conduction band (CB) is occupied by the large, medium and small amounts of V-4d, O-2p and I-5p states, respectively. Hence, V, I and O atoms dominated the bandgap of $K_3V_2O_3F_4(IO_3)_3$.

Calculations of the birefringent properties of $K_3V_2O_3F_4(IO_3)_3$ were performed (Fig. 3b). The birefringence of $K_3V_2O_3F_4(IO_3)_3$ is calculated to be 0.158 @ 2050 nm, which is large enough to achieve phase-matching. Compared to previously reported metal vanadium iodate-fluorides including α-Ba$_2$[VO$_2$F$_2$(IO$_3$)$_2$](IO$_3$) and CsVO$_2$F(IO$_3$),[34,35] reduction of the structural dimension from the 3D [VO$_2$F(IO$_3$)]$^-$ framework to the 0D unit produces a large enhancement of optical anisotropy. Hence, the birefringence of $K_3V_2O_3F_4(IO_3)_3$ (0.158 @ 2050 nm) and α-Ba$_2$[VO$_2$F$_2$(IO$_3$)$_2$](IO$_3$) (0.200 @ 2050 nm) is far larger than that of CsVO$_2$F(IO$_3$) (0.04 @ 2050 nm).[34,45] Additionally, the birefringence of $K_3V_2O_3F_4(IO_3)_3$ at 1064 nm (0.168) is also larger

than that of K$_5$(W$_3$O$_9$F)(IO$_3$) (0.083 @ 1064 nm),[16] α-Ba$_2$[GaF$_4$(IO$_3$)$_2$](IO$_3$) (0.126 @ 1064 nm)[45] and γ-KMoO$_3$(IO$_3$) (0.087 @ 1064 nm)[46] with Λ-shaped motifs.

The specific SHG contributions from the respective groups have also been studied by DFT calculations. The calculated non-vanishing independent SHG tensors are $d_{15} = 15.23$ pm V^{-1}, $d_{24} = 1.98$ pm V^{-1}, and $d_{33} = 11.46$ pm V^{-1}. Notably, the largest SHG d_{15} tensor is 15.23 pm V^{-1}, which is larger than that of CsVO$_2$F(IO$_3$) (13.9 pm V^{-1}), α-Ba$_2$[VO$_2$F$_2$(IO$_3$)$_2$](IO$_3$) ($d_{31} = 4.68$ pm V^{-1}), γ-KMoO$_3$(IO$_3$) ($d_{11} = 5.76$ pm V^{-1}) and α-Ba$_2$[GaF$_4$(IO$_3$)$_2$](IO$_3$) ($d_{33} = 1.93$ pm V^{-1}).[34,35,45,46] The calculated results are roughly consistent with the SHG effect magnitude: $K_3V_2O_3F_4(IO_3)_3$ (1.3 × KTP) > CsVO$_2$F(IO$_3$) (1.1 × KTP) = γ-KMoO$_3$(IO$_3$) (1.1 × KTP) > α-Ba$_2$[VO$_2$F$_2$(IO$_3$)$_2$](IO$_3$) (0.7 × KTP) > α-Ba$_2$[GaF$_4$(IO$_3$)$_2$](IO$_3$) (0.4 × KTP).[34,35,45,46]

Furthermore, the SHG origins of $K_3V_2O_3F_4(IO_3)_3$ were investigated and the SHG density maps are shown in Fig. 3c and d. The dominating SHG source is the non-bonding O-2p states in the VB, whereas, in the CB, the empty V-3d states, O-2p states from V–O–I bridges, and few F-2p states define the SHG response of $K_3V_2O_3F_4(IO_3)_3$. The SHG contribution percentages of VO$_4$F$_2$, VO$_3$F$_2$, and IO$_3$ groups are 32.5%, 15.6%, and 50.2%, respectively. Accordingly, we suggest that assembling different vanadium oxide fluoride motifs and iodate anions produces a synergistic effect, and led to a strong SHG response for $K_3V_2O_3F_4(IO_3)_3$.

Conclusions

In conclusion, explorations of metal vanadium iodate-fluorides afforded $K_3V_2O_3F_4(IO_3)_3$ with a 0D [V$_2$O$_3$F$_4$(IO$_3$)$_3$]$^{3-}$ polyanion, which is composed of three types of SHG functional groups (VO$_4$F$_2$ octahedron, VO$_3$F$_2$ square pyramid, and IO$_3$ triangular pyramid). Interestingly, $K_3V_2O_3F_4(IO_3)_3$ exhibits a very strong SHG effect (1.3 × KTP) and a large birefringence (0.158 @ 2050 nm). Therefore, $K_3V_2O_3F_4(IO_3)_3$ is a promising SHG crystal. Further studies to explore new metal iodate SHG materials containing two different d^0-TM centered polyhedra are in progress.

Data availability

All data included in this study are available upon request by contact with the corresponding author.

Author contributions

Chen Jin: conceptualization, methodology, writing – original draft, data curation, visualization, writing – review & editing; Li Yi-Lin, Chen Yan and Chen Qian-Qian: data curation; Hu Chun-Li: formal analysis, software; Mao Jiang-Gao: supervision.

Conflicts of interest
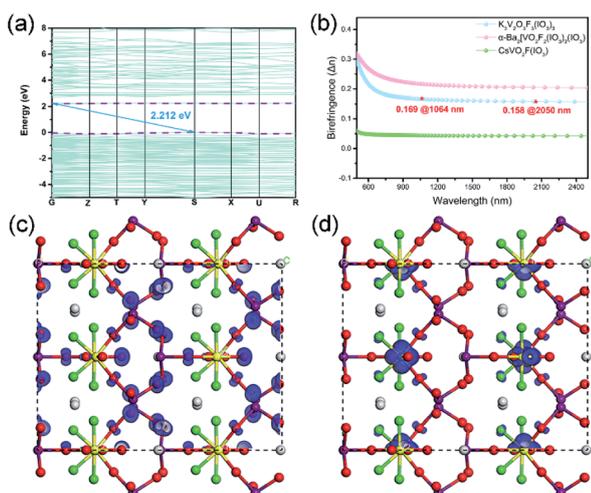
There are no conflicts to declare.

Fig. 3 The calculated band structure (a), the birefringence (b), and the SHG density plots: (c) VB and (d) CB for $K_3V_2O_3F_4(IO_3)_3$.

Acknowledgements

Notes and references

1 M. Mutailipu, K. R. Poeppelmeier and S. Pan, *Chem. Rev.*, 2021, **121**, 1130–1202.

2 K. M. Ok, E. O. Chi and P. S. Halasyamani, *Chem. Soc. Rev.*, 2006, **35**, 710–717.

3 G. Zou and K. M. Ok, *Chem. Sci.*, 2020, **11**, 5404–5409.

4 X. Meng, W. Yin and M. Xia, *Coord. Chem. Rev.*, 2021, **439**, 213916.

5 M. Zhang, D. An, C. Hu, X. Chen, Z. Yang and S. Pan, *J. Am. Chem. Soc.*, 2019, **141**, 3258–3264.

6 C. Wu, T. Wu, X. Jiang, Z. Wang, H. Sha, L. Lin, Z. Lin, Z. Huang, X. Long, M. G. Humphrey and C. Zhang, *J. Am. Chem. Soc.*, 2021, **143**, 4138–4142.

7 C. Jin, X. Shi, H. Zeng, S. Han, Z. Chen, Z. Yang, M. Mutailipu and S. Pan, *Angew. Chem., Int. Ed.*, 2021, **60**, 20469–20475.

8 X. Zhang, L. Kang, P. Gong, Z. Lin and Y. Wu, *Angew. Chem., Int. Ed.*, 2021, **60**, 6386–6390.

9 J. Shi, Y. He, F. Liang, X. Zhang, D. Xu, J. Yao, G. Zhang, Z. Hu, J. Yao and Y. Wu, *J. Mater. Chem. C*, 2020, **8**, 4226–4233.

10 J. Chen, C. L. Hu, F. Kong and J. G. Mao, *Acc. Chem. Res.*, 2021, **54**, 2775–2783.

11 C. L. Hu and J. G. Mao, *Coord. Chem. Rev.*, 2015, **288**, 1–17.

12 C. Sun, B. Yang and J. Mao, *Sci. China: Chem.*, 2011, **54**, 911.

13 H.-Y. Chang, S.-H. Kim, P. S. Halasyamani and K. M. Ok, *J. Am. Chem. Soc.*, 2009, **131**, 2426–2427.

14 C. F. Sun, C. L. Hu, X. Xu, J. B. Ling, T. Hu, F. Kong, X. F. Long and J. G. Mao, *J. Am. Chem. Soc.*, 2009, **131**, 9486–9487.

15 R. E. Sykora, K. M. Ok, P. S. Halasyamani and T. E. Albrecht-Schmitt, *J. Am. Chem. Soc.*, 2002, **124**, 1951–1957.

16 C. Wu, L. Lin, X. Jiang, Z. Lin, Z. Huang, M. G. Humphrey, P. S. Halasyamani and C. Zhang, *Chem. Mater.*, 2019, **31**, 10100–10108.

17 C. Huang, C. L. Hu, X. Xu, B. P. Yang and J. G. Mao, *Inorg. Chem.*, 2013, **52**, 11551–11562.

18 J. Chen, C.-L. Hu, F.-F. Mao, X.-H. Zhang, B.-P. Yang and J.-G. Mao, *Chem. Sci.*, 2019, **10**, 10870–10875.

19 H. Liu, X. Jiang, X. Wang, L. Yang, Z. Lin, Z. Hu, X.-G. Meng, X. Chen and J. Qin, *J. Mater. Chem. C*, 2018, **6**, 4698–4705.

20 S. D. Nguyen, J. Yeon, S. H. Kim and P. S. Halasyamani, *J. Am. Chem. Soc.*, 2011, **133**, 12422–12425.

21 F. F. Mao, C. L. Hu, X. Xu, D. Yan, B. P. Yang and J. G. Mao, *Angew. Chem., Int. Ed.*, 2017, **56**, 2151–2155.

22 H. Liu, Q. Wu, X. Jiang, Z. Lin, X. Meng, X. Chen and J. Qin, *Angew. Chem., Int. Ed.*, 2017, **56**, 9492–9496.

23 M. Zhang, X. Su, M. Mutailipu, Z. Yang and S. Pan, *Chem. Mater.*, 2017, **29**, 945–949.

24 J. Chen, C.-L. Hu and J.-G. Mao, *Sci. China Mater.*, 2021, **2**, 400–407.

25 M. Gai, Y. Wang, T. Tong, Z. Yang and S. Pan, *Inorg. Chem.*, 2020, **59**, 4172–4175.

26 M. Gai, T. Tong, Y. Wang, Z. Yang and S. Pan, *Chem. Mater.*, 2020, **32**, 5723–5728.

27 H. Fan, C. Lin, K. Chen, G. Peng, B. Li, G. Zhang, X. Long and N. Ye, *Angew. Chem., Int. Ed.*, 2020, **59**, 5268–5272.

28 T. Abudouwufu, M. Zhang, S. Cheng, H. Zeng, Z. Yang and S. Pan, *Chem. Mater.*, 2020, **32**, 3608–3614.

29 J. Chen, C.-L. Hu, F.-F. Mao, B.-P. Yang, X.-H. Zhang and J.-G. Mao, *Angew. Chem., Int. Ed.*, 2019, **58**, 11666–11669.

30 X. Su, Y. Chu, Z. Yang, B.-H. Lei, C. Cao, Y. Wang, Q. Liu and S. Pan, *J. Phys. Chem. C*, 2020, **124**, 24949–24956.

31 X. Su, Z. Yang, G. Han, Y. Wang, M. Wen and S. Pan, *Dalton Trans.*, 2016, **45**, 14394–14402.

32 A. K. Paidi, P. W. Jaschin, K. B. R. Varma and K. Vidyasagar, *Inorg. Chem.*, 2017, **56**, 12631–12640.

33 J. Yeon, S.-H. Kim and P. S. Halasyamani, *Inorg. Chem.*, 2010, **49**, 6986–6993.

34 J. Chen, C.-L. Hu, X.-H. Zhang, B.-X. Li, B.-P. Yang and J.-G. Mao, *Angew. Chem., Int. Ed.*, 2020, **59**, 5381–5384.

35 H. Yu, M. L. Nisbet and K. R. Poeppelmeier, *J. Am. Chem. Soc.*, 2018, **140**, 8868–8876.

36 B. P. Yang, C. L. Hu, X. Xu, C. Huang and J. G. Mao, *Inorg. Chem.*, 2013, **52**, 5378–5384.

37 C. Huang, C.-L. Hu, X. Xu, B.-P. Yang and J.-G. Mao, *Dalton Trans.*, 2013, **42**, 7051–7058.

38 C. F. Sun, C. L. Hu, X. Xu, B. P. Yang and J. G. Mao, *J. Am. Chem. Soc.*, 2011, **133**, 5561–5572.

39 B. P. Yang, C. L. Hu, X. Xu, C. F. Sun, J. H. Zhang and J. G. Mao, *Chem. Mater.*, 2010, **22**, 1545–1550.

40 C. F. Sun, T. Hu, X. Xu and J. G. Mao, *Dalton Trans.*, 2010, **39**, 7960–7967.

41 X. A. Chen, L. Zhang, X. A. Chang, H. G. Zang and W. Q. Xiao, *Acta Crystallogr., Sect. C: Cryst. Struct. Commun.*, 2006, **62**, i76–i78.

42 R. E. Sykora, K. M. Ok, P. S. Halasyamani, D. M. Wells and T. E. Albrecht-Schmitt, *Chem. Mater.*, 2002, **14**, 2741–2749.

43 P. Kubelka and F. Munk, *Z. Tech. Phys.*, 1931, **12**, 259–274.

44 S. K. Kurtz and T. T. Perry, *J. Appl. Phys.*, 1968, **39**, 3798–3813.

45 J. Chen, C.-L. Hu, F.-F. Mao, J.-H. Feng and J.-G. Mao, *Angew. Chem., Int. Ed.*, 2019, **58**, 2098–2102.

46 J. Chen, C.-L. Hu, Y.-L. Li, Q.-Q. Chen, B.-X. Li and J.-G. Mao, *J. Alloys Compd.*, 2021, 162547, DOI: 10.1016/j.jallcom.2021.162547.

47 R. H. Blessing, *Acta Crystallogr., Sect. A: Found. Crystallogr.*, 1995, **51**, 33–38.

48 G. M. Sheldrick, *Acta Crystallogr., Sect. C: Struct. Chem.*, 2015, **71**, 3–8.

49 A. Spek, *J. Appl. Crystallogr.*, 2003, **36**, 7–13.

50 H. D. Flack and G. Bernardinelli, *The use of X-ray crystallography to determine absolute configuration*, 2008, vol. 20, pp. 681–690.

51 M. Segall, P. J. Lindan, M. a. Probert, C. J. Pickard, P. J. Hasnip, S. Clark and M. Payne, *J. Phys.: Condens. Matter*, 2002, **14**, 2717.

52 V. Milman, B. Winkler, J. White, C. Pickard, M. Payne, E. Akhmatskaya and R. Nobes, *Int. J. Quantum Chem.*, 2000, **77**, 895–910.

53 J. P. Perdew, K. Burke and M. Ernzerhof, *Phys. Rev. Lett.*, 1996, **77**, 3865.

54 J. Lin, A. Qteish, M. Payne and V. Heine, *Phys. Rev. B: Condens. Matter Mater. Phys.*, 1993, **47**, 4174.

55 C. Aversa and J. Sipe, *Phys. Rev. B: Condens. Matter Mater. Phys.*, 1995, **52**, 14636.

56 S. N. Rashkeev, W. R. Lambrecht and B. Segall, *Phys. Rev. B: Condens. Matter Mater. Phys.*, 1998, **57**, 3905.

57 J. Lin, M.-H. Lee, Z.-P. Liu, C. Chen and C. J. Pickard, *Phys. Rev. B: Condens. Matter Mater. Phys.*, 1999, **60**, 13380.

58 L. Lin, X. Jiang, C. Wu, Z. Lin, Z. Huang, M. G. Humphrey and C. Zhang, *Dalton Trans.*, 2021, **50**, 7238–7245.